

Experimental testing of two short-fiber reinforced composites: PPA-GF33 and PPS-GF40

Dan Micota¹  | Alexandru Isaincu²  | Liviu Marşavina¹ 

¹Department of Mechanics and Strength of Materials, Politehnica University of Timișoara, Timișoara, Romania

²Department of Steel Structures and Structural Mechanics, Politehnica University of Timișoara, Timișoara, Romania

Correspondence

Alexandru Isaincu, Department of Steel Structures and Structural Mechanics, Politehnica University of Timișoara, Ioan Curea, No. 1, Timișoara 300223, Romania.
Email: alexandru.isaincu@student.upt.ro

Abstract

This paper presents an experimental testing of two short-fiber reinforced composites (SFRC). The two materials are a polyphthalamide with 33% glass fiber inclusion (PPA-GF33) and a polyphenylene sulfide with 40% glass fiber inclusion. Rectangular plates were obtained from these two materials by injection molding. Specimens, type 1BA, according to ISO 527-2, were cut out with orientations of 0°, 15°, 30°, 45°, 60°, and 90°, with respect to the longitudinal direction of the plate. The cutting was conducted using a CNC water jet machine. Tension tests were performed at room temperature, in order to determine the mechanical behavior. Results are presented in the form of stress–strain curves, considering different orientations of the specimens. The experimental results were processed in order to assess the differences that appear due to fiber orientation. A comparison between the two materials was performed in terms of Young's modulus, tensile strength, and tensile strain. The experimental data were used to calibrate the Tsai–Hill fracture criterion.

KEYWORDS

fiber orientation, polyphenylene sulfide, polyphthalamide, short-fiber reinforced composites

1 | INTRODUCTION

The use of short fiber reinforced polymers (SFRP) is constantly increasing because of the advantages that this type of material is providing. One of the most important advantage is that they are produced by injection molding method. This is a very attractive process because it allows rapid processing, high volumes that can be produced, and complex geometric shapes that can be obtained without expensive post-production machining. The second advantage represents their lightweight. This makes them suitable for all kinds of applications in many industries. The understanding and characterization of SFRP, from a mechanical point of view, are a continuous need for the industry to develop better products and more cost efficient.

One disadvantage of SFRP is that they present anisotropic behavior. This makes them harder to be characterized and requires more advanced testing procedures.

The principal factor that affects the mechanical properties of SFRP is the fiber orientation. There are many factors that affect the fiber orientation such as injection point position, injection speed, injection pressure, mold temperature, fiber content, part geometry, and overall thickness.^{1–4} Many studies are conducted to present the effects of fiber orientation on to the mechanical response of composite materials.^{5–21}

Many of the material suppliers commonly classify thermoplastic polymers using a pyramid like structure.^{22,23} The faces of the pyramid are represented by the polymer structure (amorphous or semi-crystalline), and the height usually

corresponds to an increase in cost, performance and difficulty of forming. At the bottom, we have the standard plastics (used for high consumption applications), engineering plastics (applications that require at least one advanced characteristic), and high-performance plastics (applications that demand higher temperatures and mechanical properties). Some variations of this classification can be seen that place ultra-performance plastics, such as polyetheretherketone (PEEK), at the top.

2 | MATERIALS

Two thermoplastic materials are studied in this paper. Both are provided by Solvay Group. One of the materials is a polyphthalamide (PPA) with glass fiber inclusions of 33% (GF33). In the market, this material can be found under the trade name of Amodel AE-4133. The second material is a polyphenylene sulfide (PPS) with glass fiber inclusions of 40% (GF40). In the market, this material can be found under the trade name of Ryton R-4-270. They both have a semi-crystalline structure and are included in the high-performance polymers. This puts them on top of the previous mentioned pyramid. The two materials are widely used in the automotive industry.

3 | EXPERIMENTAL TESTING

The materials were delivered as rectangular plates, with nominal measures of 100 mm length, 80 mm width, and 2 mm thickness. The plates were obtained using injection molding process. These rectangular plates were cut from a longer plate, having a length of 300 mm, in order to obtain a good orientation of the fibers. Only the last third of this long plate was delivered for testing.

Dog bone specimens were cut via water jet machine according to ISO 527-2.²⁴ Due to the small dimensions of the plates (100 mm × 80 mm × 2 mm), probes type 1BA were used, see Figure 1B. Because of the water jetting process, rough surfaces resulted. All probes were sanded on their cut sections to reduce the number and severity of stress concentrators. To have specimens with a uniform fiber orientation distribution, only one dog bone specimen was cut from the middle of the plate for 15°, 30°, 45°, and 60° orientation. For 0° and 90° orientation, two specimens were cut from each plate. All these orientations can be seen in Figure 1A. A number of five specimens were tested for all orientations. In the end, a set of 60 (30 for PPA-GF33 and 30 for PPS-GF40) dog bone specimens were investigated.

All tensile tests were performed on an Instron 8874 biaxial servo-hydraulic testing system, fit for axial, torsion, and combined axial-torsion tests. Only the axial static capabilities of the machine were used this time. The machine is equipped with Series 2742-30 kN fatigue rated hydraulic wedge grips, which allow for precise control of tightening pressure in order to avoid specimen's slippage. Also, the design of the grips automatically compensates for changes in specimen's thickness to maintain the grip force constant during the tests. The tests have also benefitted of the Instron

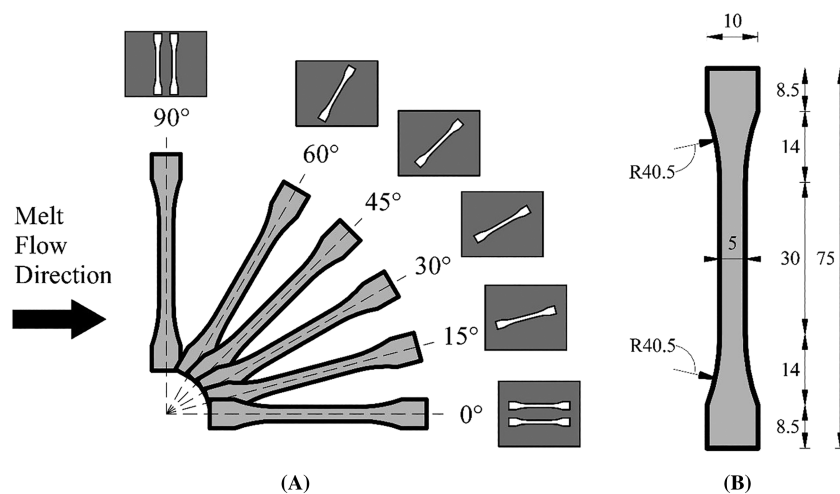


FIGURE 1 (A) Specimen orientations to the melt flow direction (θ angle) and (B) dog bone specimen dimensions (thickness 2 mm)

SVE1 (Standard Video Extensometer 1) 2663-822, non-contacting video extensometer, which records accurate axial strain data of the specimens during testing, until breaking point.

The tensile tests were conducted according to ISO 527-1.²⁵ Only room temperature was considered in this phase. A testing speed of 5 mm/min was used. In all cases, during the tensile tests, no necking was observed, and the fracture is quasi-brittle.

4 | RESULTS

The results in terms of engineering stress and strain are presented in Figure 2 for both materials (PPA-GF33 and PPS-GF40). A typical response for SFRP was obtained. For both materials, the influence of the fiber orientation is substantial. To better compare the results, the same scale was kept, both for stress axis and strain axis. Five tests were performed for all the considered directions, only one representative curve was plotted in the graphs.

All the results in terms of mean values, standard deviation, and coefficient of variation for Young's modulus, tensile strength, and strain at break function of testing angle are presented in Table 1.

Comparing the materials from a strain point of view, we can identify that PPA-GF33 has a more ductile behavior in comparison with PPS-GF40. Usually, the ductility increases with the angle of testing (θ). This behavior is more evident for PPA-GF33. Exception makes the 90° angle that has a smaller strain at break compared with 60° , thus changing the increasing trend. For PPS-GF40, an increase in ductility up to the 30° orientation is obtained. After this angle, the ductility starts to decrease until 90° . Even if this decrease appears, the differences in strain in this range (between 30° and 60°) are minimal (around 7%). The fiber content also influences the ductility. A higher fiber content will lead to a decrease in ductility, with an increase in rigidity and strength.^{3,6}

For both materials, the stress at break is decreasing with the angle. The strength at break for 90° is approximately half of the strength obtained at 0° . This behavior is similar for both PPA-GF33 and PPS-GF40. Comparing the two materials, Figure 2 shows the results function of angle of testing. Smaller differences can be seen at the two extremes (0° and 90°). The difference is around 4%. In between this range, differences up to 12% can be seen.

The tensile modulus was computed according to ISO 527-1,²⁵ using the chord slope methodology. The strain range considered for this method is 0.05%–0.25%. In order to obtain the stresses at these precise strain values, linear interpolations were performed between the test data points. The results are presented in Table 1 and Figure 4. We can see that the variation of the Young's modulus is similar for both materials (it decreases with the orientation). Percentwise, this decrease is roughly 50% (from the 0° to 90° orientation). The PPS-GF40 is, on average, with 35% stiffer in comparison with the PPA-GF33.

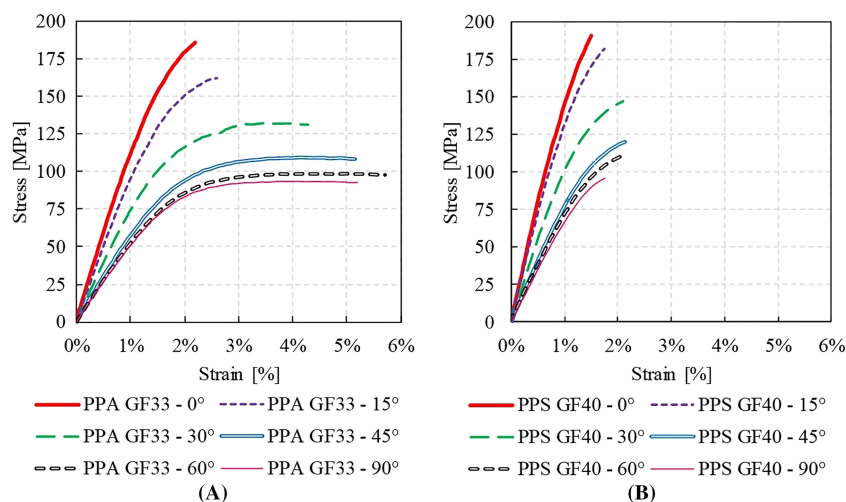


FIGURE 2 Engineering stress–strain curves obtained from tensile tests considering different orientation for (A) PPA-GF33 and (B) PPS-GF40

TABLE 1 Mean values (μ), standard deviation (σ), and coefficient of variation (CV) for Young's modulus, tensile strength, and strain at break function of orientations for PPA-GF33 and PPS-GF40

Mat.	θ (°)	Young's modulus			Tensile strength			Strain at break		
		μ (MPa)	σ (MPa)	CV (%)	μ (MPa)	σ (MPa)	CV (%)	μ (%)	σ (%)	CV (%)
PPA GF33	0	11,698	± 314	2.7	186	± 1	0.8	2.20	± 0.14	6.4
	15	10,023	± 269	2.7	163	± 2	1.2	2.74	± 0.18	6.6
	30	7930	± 467	5.9	131	± 3	2.6	4.18	± 0.27	6.5
	45	6523	± 43	0.7	110	± 1	0.7	5.13	± 0.43	8.3
	60	5626	± 144	2.6	100	± 1	0.8	5.47	± 0.23	4.1
	90	5621	± 249	4.4	96	± 2	1.6	5.02	± 0.35	7.0
PPS GF40	0	15,923	± 431	2.7	195	± 3	1.6	1.56	± 0.07	4.7
	15	14,161	± 177	1.3	177	± 5	2.9	1.67	± 0.09	5.4
	30	10,529	± 472	4.5	147	± 2	1.4	2.22	± 0.09	4.0
	45	8813	± 277	3.1	122	± 2	2.0	2.16	± 0.06	2.9
	60	7544	± 168	2.2	108	± 2	2.0	2.06	± 0.08	4.0
	90	7376	± 238	3.2	100	± 3	2.8	1.83	± 0.08	4.5

The experimental data were used to calibrate the Tsai–Hill fracture criterion.²⁶ According to previous studies,^{11,27} the failure criteria for transversal isotropic material under plane stress state have the following expression:

$$\frac{\sigma_1^2}{T_1^2} + \frac{\sigma_2^2}{T_2^2} - \frac{\sigma_1 \cdot \sigma_2}{T_1^2} + \frac{\tau_{12}^2}{S_{12}^2} = 1 \quad (1)$$

In Equation 1, T_1 and T_2 are defined as the tensile strengths of the material in the principal directions (T_1 corresponds to the 0° orientation and will be denoted as T_{0° , T_2 corresponds to the 90° orientation and will be denoted as T_{90°) and S_{12} is defined as the shear strength.

Deriving from the same equation,¹¹ the tensile strength according with Tsai–Hill fracture criterion is

$$T_\theta = \left[\frac{\cos^4 \theta}{T_{0^\circ}^2} + \left(\frac{1}{S_{12}^2} - \frac{1}{T_{0^\circ}^2} \right) \sin^2 \theta \cos^2 \theta + \frac{\sin^4 \theta}{T_{90^\circ}^2} \right]^{-0.5} \quad (2)$$

In expression 2, T_θ represents the material strength for a certain angle orientation. Two shear strengths (S_{12}) were considered for the analytical model. Both of them are based on the tensile strength of the 45° specimen orientation (T_{45°). These shear strengths are based on the Tresca criterion according to Equation 3, respectively the von Mises criterion according to Equation 4.

$$S_{12} = \frac{T_{45^\circ}}{2} \quad (3)$$

$$S_{12} = \frac{T_{45^\circ}}{\sqrt{3}} \quad (4)$$

The strength prediction according to Tsai–Hill, for the two shear strengths considered, are presented in Figure 3, in comparison with the test results for both PPA-GF33 and PPS-GF40.

The strength prediction is more accurate if we consider the shear strength according to the von Mises criterion. For the Tresca model, the strength prediction between 45° and 75° orientation is smaller than the strength obtained at 90° orientation. This is not consistent with the obtained experimental results. For the PPA-GF33, the largest prediction

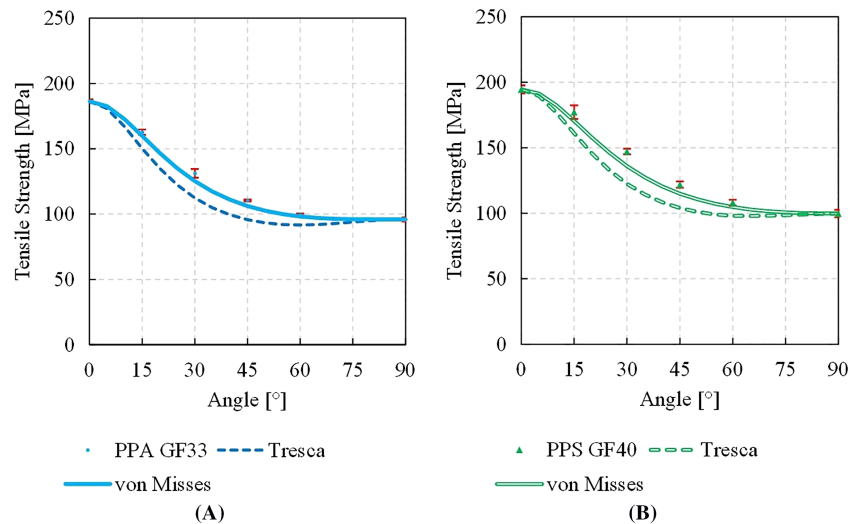


FIGURE 3 Tensile strengths test data function of orientation including the Tresca and von misses failure predictions for (A) PPA-GF33 and (B) PPS-GF40

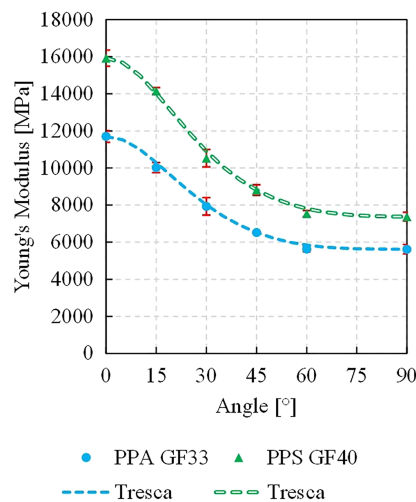


FIGURE 4 Young's modulus function of orientation including the prediction for (A) PPA-GF33 and (B) PPS-GF40

error (considering the von Misses shear strength) is with 4.5% smaller, in comparison with the test data for the 30° orientation. For the PPS-GF40, the error is 7.6%. If we consider the Tresca shear strength, the prediction error is with 14.3% and 16.8% smaller, in comparison with test data for the 30° orientation for PPA-GF33 and PPS-GF40 respectively.

The prediction in terms of rigidity, according to a previous study,¹¹ can be made using the equation:

$$E_{\theta} = \left[\frac{1}{E_{0^{\circ}}} \cos^4 \theta + \left(\frac{1}{G_{12}} - \frac{2\nu_{12}}{E_{0^{\circ}}} \right) \sin^2 \theta \cos^2 \theta + \frac{1}{E_{90^{\circ}}} \sin^4 \theta \right]^{-1} \quad (5)$$

The Poisson's ratio (ν_{12}) for the two materials is 0.37 for PPA-GF33 and 0.41 for PPS-GF40. These data were provided by the Solvay Group. The in-plane shear modulus is computed according to Equation 6, based on the Poisson's ratio and the Young's modulus for 0°, 45°, and 90° orientation.

$$G_{12} = \left(\frac{1}{E_{45^\circ}} - \frac{1}{E_{0^\circ}} - \frac{1}{E_{90^\circ}} + \frac{2\nu_{12}}{E_{0^\circ}} \right)^{-1} \quad (6)$$

A good correlation in comparison with the rigidity, computed according to the ISO-527-1,²⁵ can be seen in Figure 4. The prediction slightly overestimates the rigidity. A maximum of 3.9% overestimation can be seen for the PPA-GF33 for the 60° orientation. On average, the prediction is with 1% (for the PPS-GF40) up to 1.3% (for the PPA-GF33) stiffer than the test data.

5 | CONCLUSIONS

This paper aims to present an experimental study on the anisotropic behavior of two SFRP (PPA-GF33 and PPS-GF40) conducted at room temperature and to calibrate the Tsai–Hill failure criterion. The main conclusions that can be drawn are as follows:

- Good results were obtained from the tensile tests for both materials, if we consider the dispersion of the obtained data.
- There is a big difference in terms of rigidity (Young's modulus) and ductility (strain at break) between the two materials. On average, PPS-GF40 is less ductile, with 50%, and more rigid, with 35%, in comparison with PPA-GF33. In terms of resistance (stress at break), the differences are smaller (on average 8%).
- The rigidity prediction, based on transversal isotropic material hypothesis, under plane stress state, gives reliable results. Differences below 4% can be identified for the two materials, in comparison with the test data. Using this prediction, only three orientations need to be tested: 0°, 45°, and 90°.
- The strength prediction, based on transversal isotropic material hypothesis and Tsai–Hill strength criterion, gives good results. Differences up to 8% can be seen if we consider the von Mises shear strength. If the Tresca shear strength criterion is used, the difference increases up to 16%.
- When assessing failure prediction using the Tsai–Hill criterion for SFRC, the von Mises shear strength gives more accurate results, in comparison with Tresca shear strength.

Future directions include assessing the behavior of these two materials under temperatures (considering a temperature range from −40°C up to +120°C), calibrate a material model using Digimat software and validate the model using a mechanical test on an injected part.

ACKNOWLEDGMENTS

The project leading to this application has received funding from the European Union's Horizon 2020 research and innovation program under grant agreement no. 857124. Special thanks to Solvay Group for providing the plaques for the two materials studied and for the continuous support. Also, we would like to thank the Vitesco Technologies finite element analysis teams from Timisoara for the support and the help in cutting the specimens.

DATA AVAILABILITY STATEMENT

The data that support the findings of this study are available on request from the corresponding author. The data are not publicly available due to privacy or ethical restrictions.

ORCID

Dan Micota  <https://orcid.org/0000-0003-3222-4538>

Alexandru Isaincu  <https://orcid.org/0000-0002-0408-8826>

Liviu Marşavina  <https://orcid.org/0000-0002-5924-0821>

REFERENCES

1. Castagnet S, Nadot-Martin C, Fouchier N, Conrado E, Bernasconi A. Fatigue life assessment in notched injection-molded specimens of a short-glass fiber reinforced polyamide 6 with different injection gate locations. *Int J Fatigue*. 2021;143:105968.

2. Huszar M, Belblidia F, Davies HM, Arnold C, Bould D, Sienz J. Sustainable injection moulding: the impact of materials selection and gate location on part warpage and injection pressure. *Sustain Mater Technol.* 2015;5:1-8.
3. Jørgensen JK, Andreassen E, Salaberger D. The effect of fiber concentration on fiber orientation in injection molded film gated rectangular plates. *Polym Compos.* Feb. 2019;40(2):615-629.
4. Holmström PH, Hopperstad OS, Clausen AH. Anisotropic tensile behaviour of short glass-fibre reinforced polyamide-6. *Compos Part C Open Access.* Oct. 2020;2:100019.
5. Bernasconi A, Davoli P, Basile A, Filippi A. Effect of fibre orientation on the fatigue behaviour of a short glass fibre reinforced polyamide-6. *Int J Fatigue.* 2007;29(2):199-208.
6. Ogierman W, Kokot G. A study on fiber orientation influence on the mechanical response of a short fiber composite structure. *Acta Mech.* 2016;227(1):173-183.
7. Micota D, Isaincu A, Marsavina L. Micromechanical modeling of glass fiber reinforced plastic material. *Mater Today Proc.* 2021;45(5):4330-4336.
8. Şerban DA, Weissenborn O, Geller S, Marşavina L, Gude M. Evaluation of the mechanical and morphological properties of long fibre reinforced polyurethane rigid foams. *Polym Test.* Feb. 2016;49:121-127.
9. Şerban DA, Marsavina L, Silberschmidt V. Behaviour of semi-crystalline thermoplastic polymers: experimental studies and simulations. *Comput Mater Sci.* 2012;52(1):139-146.
10. Hassan A, Yahya R, Yahaya AH, Tahir ARM, Hornsby PR. Tensile, impact and fiber length properties of injection-molded short and long glass fiber-reinforced polyamide 6,6 composites. *J Reinf Plast Compos.* 2004;23(9):969-986.
11. Zhao Y, Chen Y, Zhou Y. Novel mechanical models of tensile strength and elastic property of FDM AM PLA materials: experimental and theoretical analyses. *Mater Des.* 2019;181:108089.
12. Isaincu A, Micota D, Ungureanu V, Marşavina L. Numerical investigation on the influence of fiber orientation mapping procedure to the mechanical response of short-fiber reinforced composites using Moldflow, Digimat and Ansys software. *Mater Today Proc.* 2021;45(5):4304-4309.
13. Oseli A, Prodan T, Susić E, Slemenik Perše L. The effect of short fiber orientation on long term shear behavior of 40% glass fiber reinforced polyphenylene sulfide. *Polym Test.* 2020;81:106262.
14. Lohr C, Beck B, Henning F, Weidenmann KA, Elsner P. Process comparison on the microstructure and mechanical properties of fiber-reinforced polyphenylene sulfide using MuCell technology. *J Reinf Plast Compos.* Aug. 2018;37(15):1020-1034.
15. Takahashi R, Shohji I, Seki Y, Maruyama S. Effect of fiber direction and temperature on mechanical properties of short fiber-reinforced PPS. *Int Conf Electron Packag.* 2014;778-781.
16. Zhang K, Zhang G, Liu B, Wang X, Long S, Yang J. Effect of aminated polyphenylene sulfide on the mechanical properties of short carbon fiber reinforced polyphenylene sulfide composites. *Compos Sci Technol.* Jun. 2014;98:57-63.
17. Hahn H, Jerina K, Burrett P. Fiber orientation and fracture morphology in short fiber-reinforced thermoplastics. In: Newaz G, ed. *Advances in Thermoplastic Matrix Composite Materials.* West Conshohocken, PA: ASTM International; 1989:183-198.
18. Skourlis TP, Pochiraju K, Chassapis C, Manoochehri S. Structure-modulus relationships for injection-molded long fiber-reinforced polyphthalamides. *Compos Part B Eng.* 1998;29(3):309-319.
19. Ramorino G, Cecchel S, Cornacchia G. Effect of Fiber Orientation and Residual Stresses on the Structural Performance of Injection Molded Short-Fiber-Reinforced components; 2020.
20. Sawada T, Aoyama H. Effect of molding processes on multiaxial fatigue strength in short fibre reinforced polymer. *Frat Ed Integrità Strutt.* 2016;10(38):92-98.
21. Mittal M, Chaudhary R. Experimental investigation on the mechanical properties and water absorption behavior of randomly oriented short pineapple/coir fiber-reinforced hybrid epoxy composites. *Mater Res Express.* 2018;6(1):015313.
22. Zuo P, Tcharkhtchi A, Shirinbayan M, Fitoussi J, Bakir F. Overall investigation of poly (phenylene sulfide) from synthesis and process to applications — A review. *Macromol Mater Eng.* 2019;304(5):1800686.
23. Friedrich K. Polymer composites for tribological applications. *Adv Ind Eng Polym Res.* 2018;1(1):3-39.
24. ISO-527-2. Plastics - Determination of tensile properties - Part 2: Test conditions for moulding and extrusion plastics; 2012.
25. ISO-527-1. Plastics - Determination of tensile properties - Part 1: General principles; 2012.
26. Azzi VD, Tsai S. Anisotropic strength of composites. *Exper Mech.* 1965;5(9):283-288.
27. Talreja R. Analysis of failure in composite structures. In: Altenbach H, Sadowski T, eds. *Failure and Damage Analysis of Advanced Materials.* CISM Udine: Springer; 2015:255-278.

How to cite this article: Micota D, Isaincu A, Marşavina L. Experimental testing of two short-fiber reinforced composites: PPA-GF33 and PPS-GF40. *Mat Design Process Comm.* 2021;3(6):e264. <https://doi.org/10.1002/mdp2>.

[264](#)